Electronic Supplementary Information for:
Unrecognized Volatile and Semi-Volatile Organic Compounds from Brake Wear

V. Perraud,[1]† D. R. Blake,[1]† L. M. Wingen,[1] B. Barletta,[1] P. S. Bauer,[1] J. Campos,[2] M. J. Ezell,[1] A. Guenther,[2] K. N. Johnson,[1] M. Lee,[1] S. Meinardi,[1] J. Patterson,[2] E. S. Saltzman,[2] A. E. Thomas,[1] J. N. Smith[1]* and B. J. Finlayson-Pitts[1]*

[1]Department of Chemistry, University of California, Irvine, CA 92697
[2]Department of Earth System Science, University of California. Irvine, CA 92697

List of Supplementary Materials:
Materials and Methods
Figures: S1-S13
Tables: S1-S7
References

Methods:
1. C1-C10 gas measurements
Gases were sampled from the chamber port shown in Figure S1B into evacuated canisters and analyzed using GC-MS and GC-FID/EC as described in detail elsewhere.[1] The slopes of plots of each individual VOC against CO were used to obtain an average emission ratio (ER; $\Delta VOC/\Delta CO$, pptv/ppbv) for the six experiments. A total of 22 canisters per brake type were used for this analysis. The strength of the correlation varied by compound, with some showing excellent correlations while for a few there was no significant correlation. The data is summarized in Tables S3 and S4 for the ceramic and semi-metallic brakes respectively. The relative reactivities are defined as $k_{OH}[VOC]_i/k'_{OH}[CO]$, where k_{OH} is the gas phase second order rate constant for reaction with the ith VOC and k'_{OH} is the second order rate constant for the reaction of OH with CO (2.4×10^{-13} cm^3 molecule^{-1} s^{-1} at 1 atm, 298 K).

2. Sorbent tube SVOC measurements
Air samples were collected onto VOC-adsorbing sorbent tubes packed with Tenax TA and Carbograph 5TD (Markes International, Inc.). Collections were achieved by sampling the emissions from the lathe chamber at a flow rate of 200 cm^3 min^{-1} for 2.5 min (regime 2), 5 min (regime 1) or 10 min (all others). After sampling, the tubes were refrigeration-stored until analysis by thermal-desorption gas chromatography (Ultra-xr, Markes International; Model 7890B, Agilent Technologies, Inc.) coupled with mass spectrometry (Markes BenchTOF-SeV, Markes International). During thermal desorption, each tube was heated to 285°C to focus the organics on a cold trap and then heated to 290°C for release. The VOC and SVOC were transported using helium carrier gas to the gas chromatograph column at a split ratio of 4:1 (i.e. 25% of sample onto GC Column). The column flow rate was 5 mL min^{-1}, and used a constant temperature ramp of 9 °C/min to heat from 35 to 280°C resulting in a total run time of 37.2 min. The temperature was held at 35°C for 5 min at the beginning of the run and again at 280°C for 5 min at the end of the run. High resolution mass spectral information allowed for confirmation of compound identities, and quantification was achieved using a Flame Ionization Detector (FID, Agilent Technologies, Inc.) calibrated daily with a multicomponent SVOC standard (Apel-Riemer Environmental). The variability in the FID response of individual compounds was accounted for by using the effective carbon number concept.[2] Hydrocarbons with boiling points ranging from 36°C to 356°C corresponding to pentane (C5) and heneicosane (C21) respectively were measured using this technique including VOC (e. g. acetone) as well as SVOC that were efficiently trapped onto the sorbent tubes. The analysis reported in this study focuses exclusively on the SVOCs organics with 10 or more carbons for comparison with the real-time aerosol chemical composition measurement.

3. Real-time VOC measurements
Real-time measurements of VOC were performed using a high-resolution PTR-ToF-MS (PTR-8000, Ionicon Analytik).[3,4] The instrument operating principle relies on proton transfer reaction from the reagent hydronium ion (H_3O^+) to the VOC (if its affinity is higher than that of water) forming primarily $[M+H]^+$ ions. The instrument was connected directly to one of the sampling ports of the dynamometer chamber with an aluminum sampling line of ~15 cm in length. The sample (~140 cm^3 min^{-1}) from the dynamometer chamber first passed through a glass trap containing pure diiodobenzene (98%, Sigma-Aldrich) standard for mass calibration before being introduced into the PTR-MS 1/16" PEEK tubing inlet maintained at 70°C. The instrument was

operated with a drift voltage of 600 V (*Udrift*), drift temperature of 60°C (*Tdrift*) and drift pressure of ~2.25 mbar (*pdrift*), resulting in a ratio of the electric field (*E*) to the number density of the drift tube buffer gas molecules (*N*) of *E/N* ~135 Td (where 1 Td = 10^{-17} V cm^2). During experiments (in particular in regime 2), dilution air (Ultra Zero air; Praxair) was added to the PTR-MS inlet at times due to very high mixing ratios of VOC to ensure proper chemical ionization efficiency when the H_3O^+ ion was significantly depleted. All data reported here were corrected for dilution. Mass calibration was performed at the beginning of each experiment using the three reagent isotopic ions including $H_3^{18}O^+$ (*m/z* 21.0221), $^{16}O^{18}O^+$ (*m/z* 33.9935), $(H_2^{16}O)H_3^{18}O^+$ (*m/z* 39.0327) and the diiodobenzene [M+H-I]$^+$ ion at *m/z* 203.9430.[5] The data were acquired with one second time resolution continuously during the experiments. The instrument was tuned using an α-cedrene gas standard ([M+H]$^+$ at *m/z* 205.1951) and the transmission through the time-of-flight was experimentally determined using a certified mixture of 14 aromatic compounds (TO-14 mix, Linde) ranging from *m/z* 79.0542 (benzene) to *m/z* 180.9373 (trichlorobenzene).

Data analysis. Data were processed using the PTR-MS TOF Viewer software (v3.2). For each experiment, first the mass spectrum was recalibrated, and the ion signal was extracted using a nominal mass table. The goal was to initially determine an equivalent total VOC mixing ratio profile for each experiment. Mixing ratios (in ppb) of each nominal mass ion were determined using the kinetic method [6-9] and a single rate constant (*k*) for all VOC of 2.0×10^{-9} cm^3 s^{-1} in equation (1),

$$C_{ppb} = \left[\frac{10^9}{k} \cdot \frac{22400 . \mu_0 . U_{drift}}{N_A . l} \cdot \frac{T_{drift}^2[K]}{T_0^2[K]} \cdot \frac{p_0^2[mbar]}{p_{drift}^2[mbar]} \cdot \frac{Int._{nominal\,mass\,ion}}{Int._{H_3O^+}} \cdot \frac{T_{H_3O^+}}{T_{nominal\,mass\,ion}} \right] \tag{1}$$

with μ_0, the reduced mobility (2.8 cm^2 s^{-1}); N_A, Avogadro's number (6.022×10^{23}); *l*, the length of the reaction chamber (9.3 cm); p_0 and T_0 the standard pressure (1013.25 mbar) and temperature (273.15 K) respectively, $Int_{nominal\,mass\,ion}$ and $Int_{H_3O^+}$ are the signal intensities recorded at each nominal mass and for the reagent ion respectively; $T_{H_3O^+}$ and $T_{nominal\,mass\,ion}$, the transmission factors for the reagent ion and the analyte respectively. Then the total equivalent VOC mixing ratio profile for each experiment was determined by summing all nominal mass mixing ratios from *m/z* 25 to 215 (excluding *m/z* 29, 30, 32 and 37, which are related to traces amount of N_2H^+ and NO^+ in the ion source, and the reagent ions). Note that instrument background was subtracted out for each nominal mass ion prior to determining the total equivalent VOC mixing ratio.

For high resolution data analysis, individual peaks at each nominal mass ion were fitted, and mixing ratios were extracted using a proton transfer rate constant of 2.0×10^{-9} cm^3 s^{-1} and transmission coefficient determined using the TO-14 mix. Calibration of the major VOC observed was performed using several authentic standards and a dilution system. It was not possible to calibrate for all compounds identified, and for these, a large uncertainty is associated with the proton transfer rate constants,[10,11] (1.5 to ~5 × 10^{-9} cm^3 s^{-1}). The estimated uncertainty in the mixing ratios obtained by the PTRMS is thus estimated to be ±20-50%. VOC emissions from the dynamometer chamber obtained for each identified ion (given in Table S7) were further corrected for dilution and isotopic abundance. The resulting mixing ratios of each identified VOC taken at times when the WAS canisters were also collected during regime 2 were plotted

against CO mixing ratio (measured from the WAS canisters) to estimate an average emission ratio (ER, $\Delta VOC/\Delta CO$, in ppt/ppb) corresponding to the slope of these plots. Background signal for both VOC and CO were subtracted out. Data from six individual experiments performed for each brake, corresponding to a range of conditions from new to heavily worn brake pads, were used. Figure 5 shows the resulting averaged ER grouped by compound class for the ceramic brake and the semi-metallic brakes, respectively.

While recent car exhaust emissions have been documented,[12-14] and are beyond the scope of this study, five passenger vehicles were sampled with the PTR-MS. Only results for benzene (m/z 79), toluene (m/z 93), and ethylbenzene and xylenes (m/z 107) (BTEX) are presented here for comparison with the brake measurements. Acetonitrile and phenol were also quantified. Although ethylbenzene is known to fragment to some degree to m/z 79, it was not possible to account for the portion of m/z 107 that is attributed to ethylbenzene versus xylenes isomers, hence all the signal at m/z 79 was attributed to benzene, and all the signal at 107 was attributed to the sum of ethylbenzene + xylenes. The signals at m/z 79, 93 and 107 were calibrated using benzene, toluene and o-xylene respectively.

4. CO, NO and NO$_2$ measurements

Nitrogen oxide (NO) and nitrogen dioxide (NO$_2$) were measured in real time using a Thermo Scientific 42C NO-NO$_2$-NOx monitor. The sample flow rate was ~580 cm^3 min^{-1}. The monitor was calibrated prior to the campaign using certified NO (95 ppm; Scott-Marrin) and NO$_2$ (277 ppm; Scott-Marrin) gas cylinders using a series of dilutions with clean purge air. Mixing ratios of NO and NO$_2$ in the cylinders were confirmed by IR spectroscopy.

In addition to time-dependent grab-and-go CO measurements from the WAS canisters, real-time measurements using a CO monitor (Thermo Scientific 48i) were also performed. The sample flow rate was ~480 cm^3 min^{-1}. Calibration was achieved with a certified cylinder (8.99 ppm in helium; Praxair) using a series of dilution with clean purge air.

5. Particle size distribution measurements

Size distributions were recorded using a custom scanning mobility particle sizer for sizes ranging from 10 to 1000 nm. The SMPS was equipped with a ^{210}Po bipolar neutralizer, a TSI long differential mobility analyzer (DMA; model 3081), a custom blower box supplying the recirculating sheath air as well as the high voltage power supply to the DMA, and a Brechtel mixing condensation particle counter (CPC; model 1720). The ^{210}Po bipolar neutralizer used in these studies was developed by the Particle Technology Lab (PTL) at the University of Minnesota as described in Jiang et al.[15] The SMPS was operated at 0.3 L min^{-1} with a sheath air of 3 L min^{-1}. Data were recorded continuously throughout the experiment using a sequence of 60 s up and down scans. Larger particles (0.5-20 μm) were also measured using a TSI aerodynamic particle sizer (model 3321) at a flow rate of 5 L min^{-1}. Note that the first bin of the APS data is highly unreliable (particles with aerodynamic diameter < 520 nm) and was omitted from the size distribution plots.

6. Inorganic particle composition by TEM/EDS

Brake particles were collected during regime 1 onto carbon coated copper grids (Ted Pella, USA) using an electrostatic precipitator[16] for analysis by scanning transmission electron

microscopy (STEM) and electron dispersion spectroscopy (EDS). The STEM/EDS images were obtained at the UC Irvine Materials Research Institute (IMRI) facility using a JEOL JEM-2800 TEM. This instrument is equipped with a 200 kV Schottky type field emission electron source and dual 100 mm^2 Silicon Drift Detectors for x-ray analysis. The average particle size on the grids was 550 ± 250 nm for both brake pad types.

As expected, a wide variety of elements, particularly metals, was observed (Fig. S3 and S4, Table S3). In all cases, iron was the major element detected, along with smaller amounts of a number of others such as Ca, Mg, Si, Ba, K, Al and S (copper is expected to be a major contributor as well but could not be quantified due to particle collection on copper grids). As expected. the semi-metallic brakes have a larger contribution from iron.

7. Real time submicron aerosol measurements

Submicron particle composition was measured in real time with a high-resolution time-of-flight aerosol mass spectrometer (AMS, Aerodyne, Inc.).[17] The dynamometer chamber was sampled by the AMS at ~0.08 L min^{-1} through a 100 μm orifice and particles were focused with an aerodynamic lens that transmits particles of 50-1000 nm vacuum aerodynamic diameter. Particles were vaporized at 600°C, ionized by electron ionization (70 eV), and mass spectra of nonrefractory components were acquired in V-mode (m/Δm ~2000).

The AMS was calibrated using a scanning mobility particle sizer (SMPS, TSI Inc. model 3082 classifier with long DMA, model 3756 CPC). Size-selected NH_4NO_3 particles (Fisher, >98%) atomized from aqueous solutions (18.2 MΩ cm) were used to calibrate vacuum aerodynamic diameter, ionization efficiency, and mass concentration.

Data were analyzed using Igor Pro (WaveMetrics, Inc., v. 8.04) with SQUIRREL (v. 1.65C) and PIKA (v. 1.25C). High resolution mass spectra were generated after peak fitting in the range of m/z 12-200 and the relative intensities were determined for regime 2 braking sequences for the following fragment categories using nitrate-equivalent mass concentrations: hydrocarbon (C_x^+ and $C_xH_y^+$), oxygenated ($C_xH_yO_1^+$, $C_xH_yO_{>1}^+$ and HO^+), nitrogen-containing ($C_xH_yN_{1-2}^+$, $C_xH_yO_1N_{1-2}^+$, and $C_xH_yO_{>1}N_{1-2}^+$), and sulfur-containing ($C_xH_yS_{1-2}^+$ and $H_xSO_y^+$). Both $C_xH_yS_z^+$ and $H_xSO_y^+$ fragments have been shown to be generated from sulfur-containing organics.[18,19] Organosulfur compounds also form $C_xH_yO_z^+$ fragments, thus this category may be underestimated.

Mass-weighted size distributions measured by AMS indicated that particles generated from friction have much lower mass concentrations and are generally too large to transmit through the PM_1 aerodynamic lens for both ceramic and semi-metallic brakes, thus the composition determined during regime 2 represents primarily self-nucleated particles.
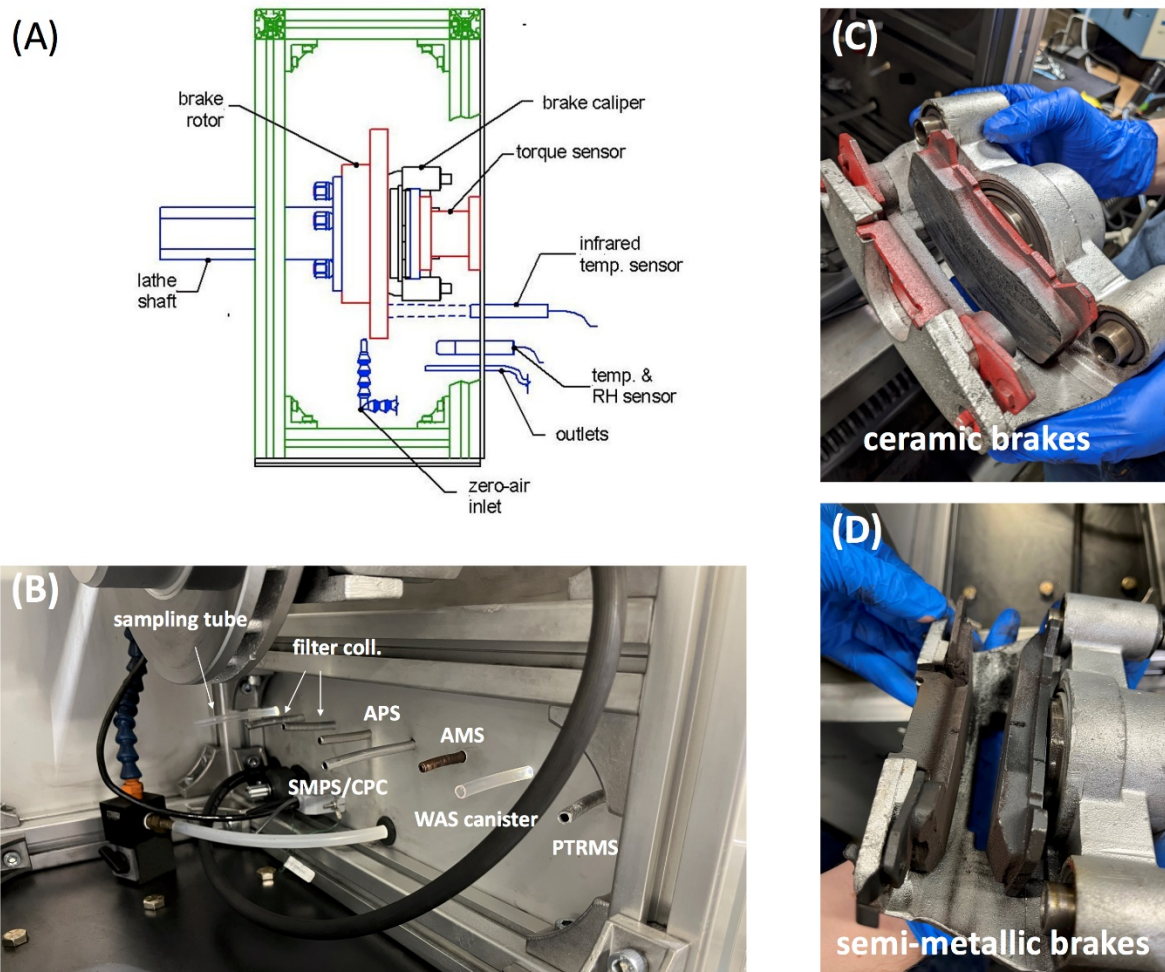
Figure S1. Details of UCI Dynamometer. (**A**) Schematic of UCI brake dynamometer; (**B**) photograph of the inside of the dynamometer chamber showing the sampling lines; (**C**) ceramic and (**D**) semi-metallic brake pads.
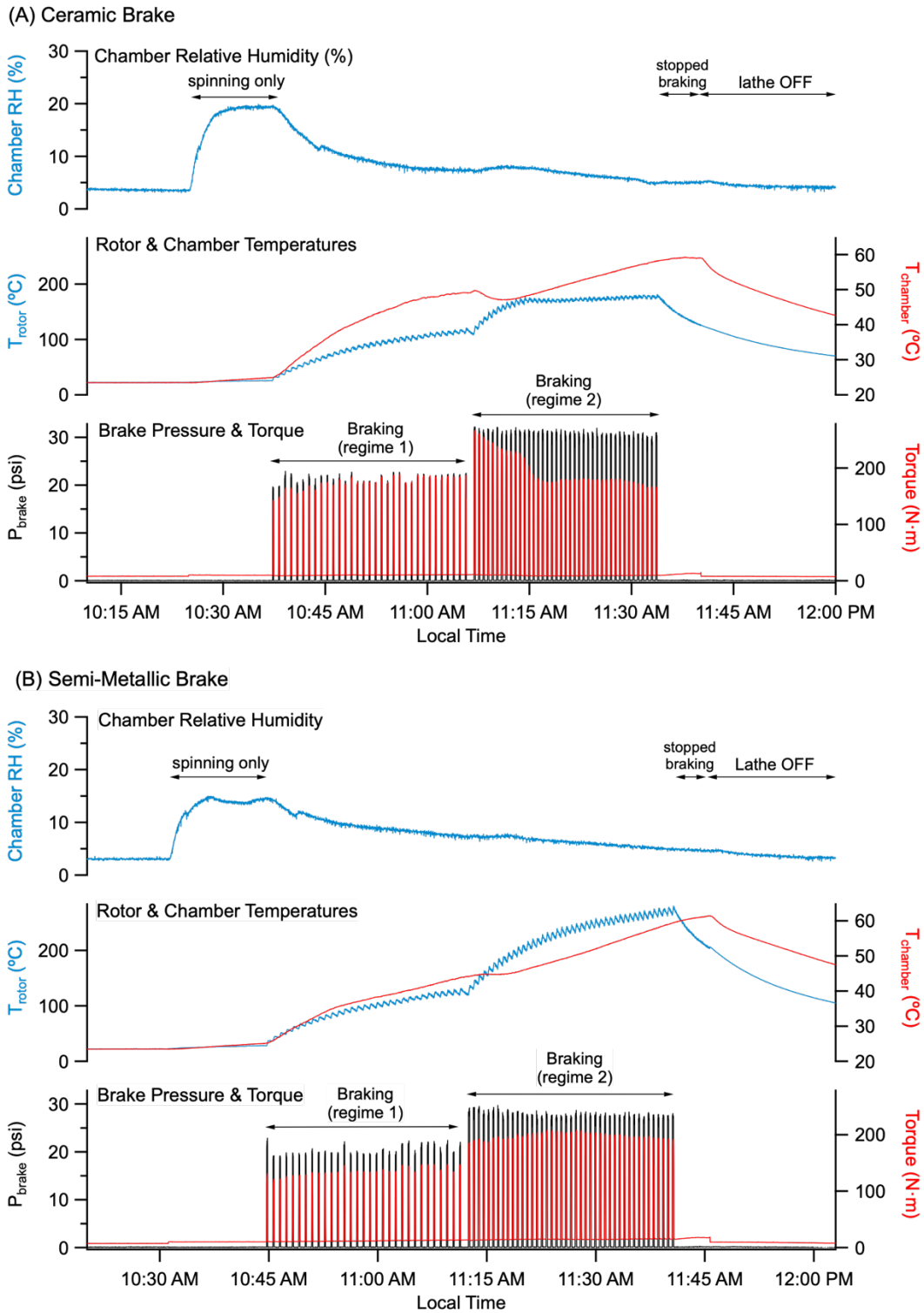
Figure S2. Braking parameters recorded during a typical dynamometer experiment for each brake pad. Braking parameters for (**A**) the ceramic brake pads, and (**B**) the semi-metallic brake pads including relative humidity in the chamber, rotor and chamber temperatures, as well as brake pressure and torque.
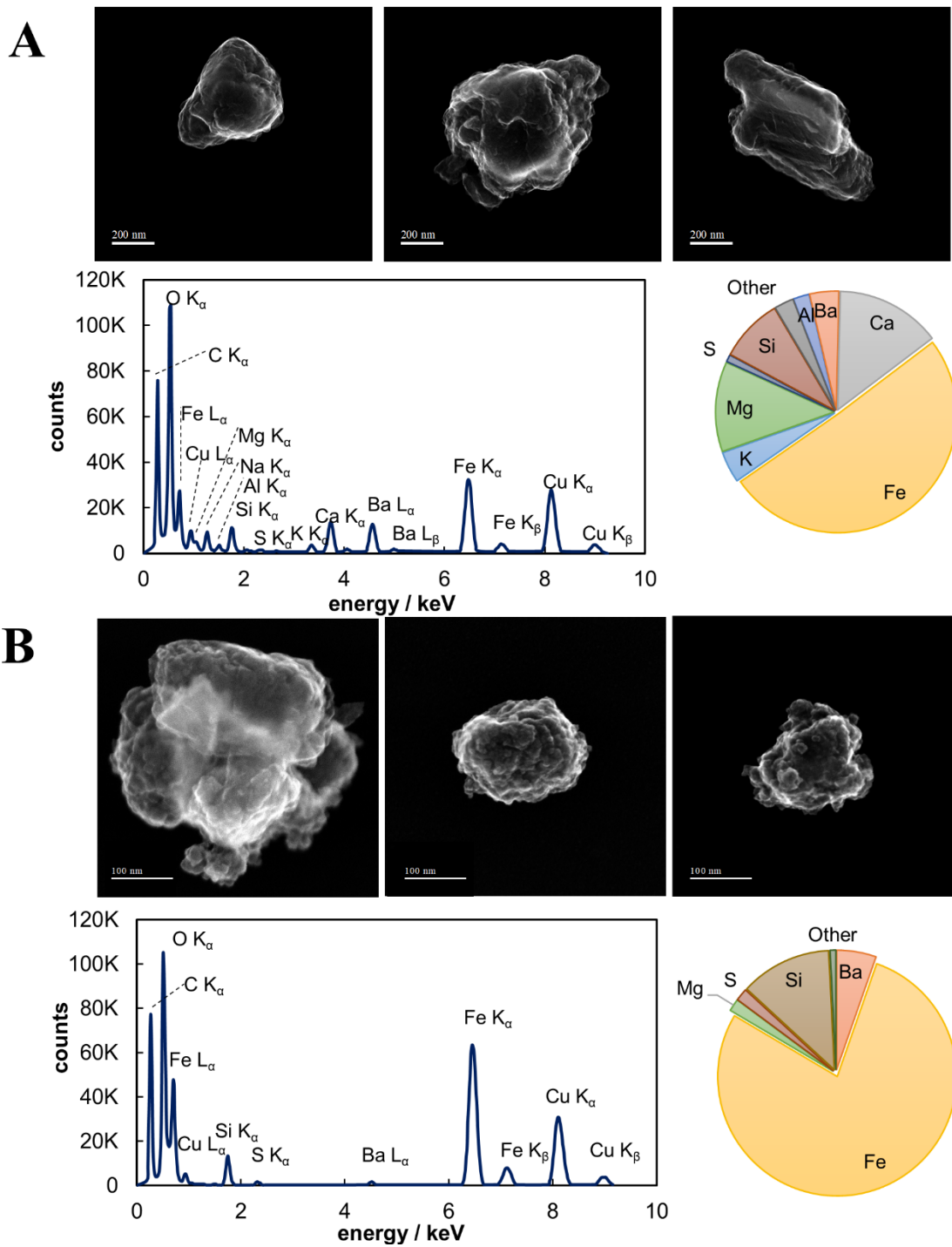
Figure S3. TEM scanning electron images from brake particles collected during a typical dynamometer experiment for each brake type. (**A**) TEM images from ceramic brake particles, and (**B**) TEM images from semi-metallic brake particles. Both panels include an average EDS spectrum from one particle and a pie chart showing the particle composition by weight percentage. Carbon and oxygen were not analyzed with this method and Cu was excluded due to its presence in the sample grid.
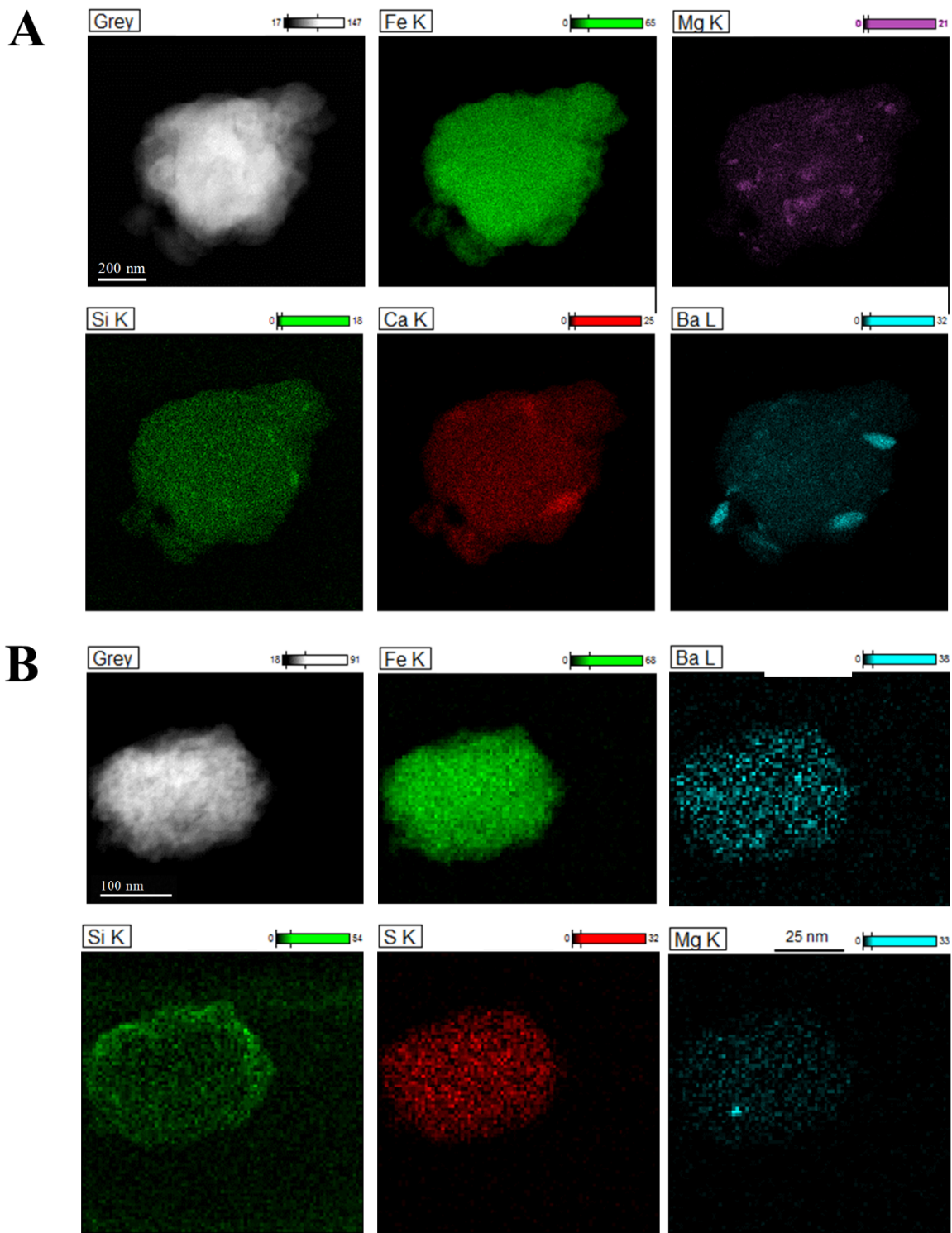
Figure S4. Representative brake pad particle EDS element maps for the five most abundant elements by weight. (**A**) Representative EDS element maps for ceramic brake particles; and (**B**) Representative EDS element maps for semi-metallic brake particles. These include a grey scale bright field image.
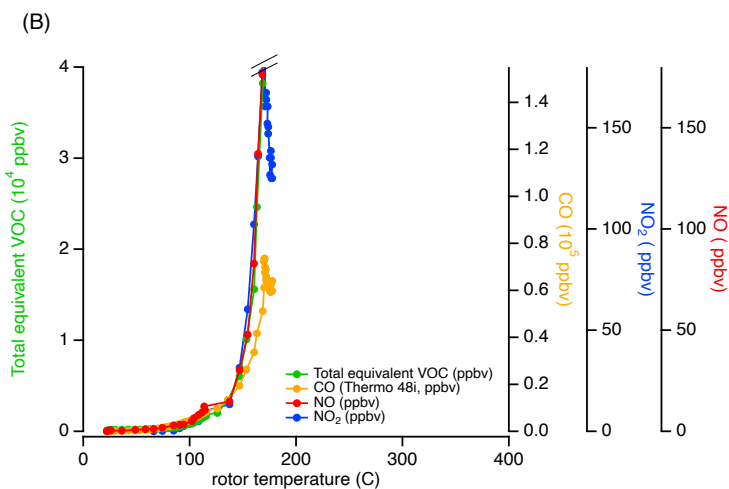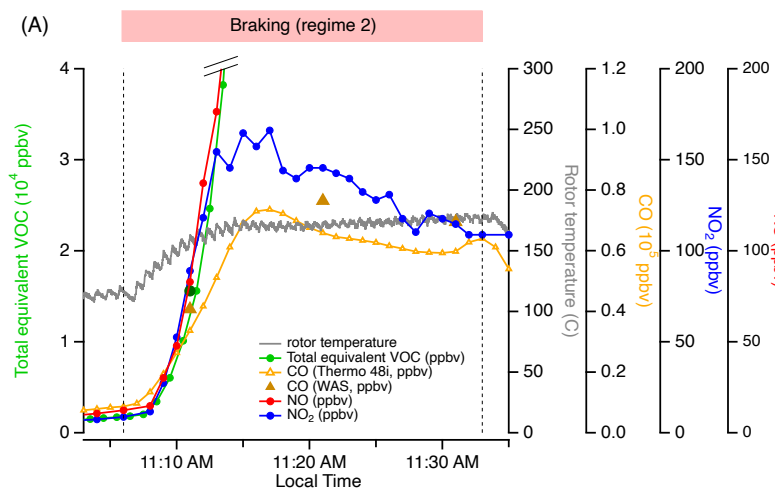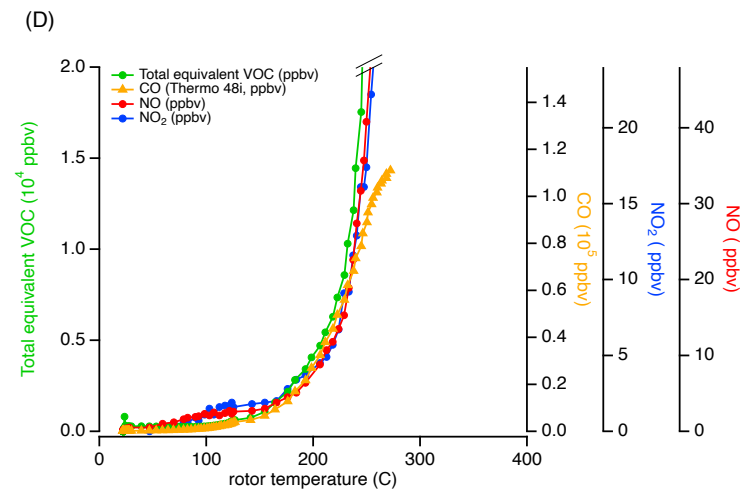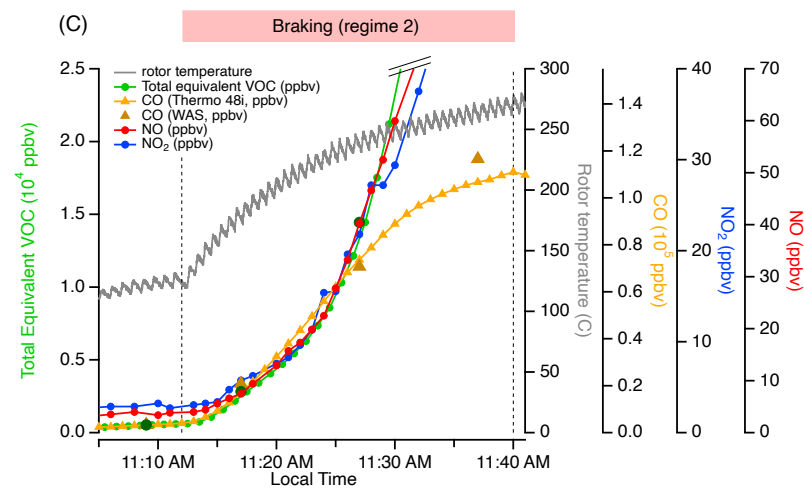
Figure S5. Time profiles of gas phase species (total equivalent VOCs, CO, NO and NO₂). Panels (A) and C) are zoomed in portions of the time profiles presented in Fig. 1 showing the onset of regime 2 period for the ceramic and semi-metallic brakes respectively. Panels (B) and (D) show the evolution of the gas phase species as a function of the rotor temperature.
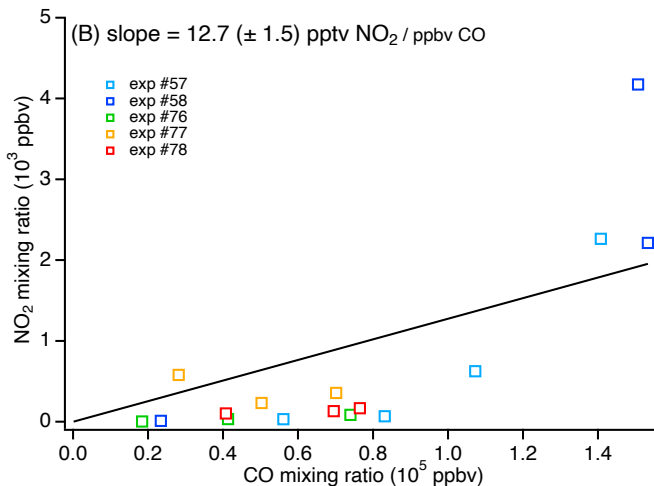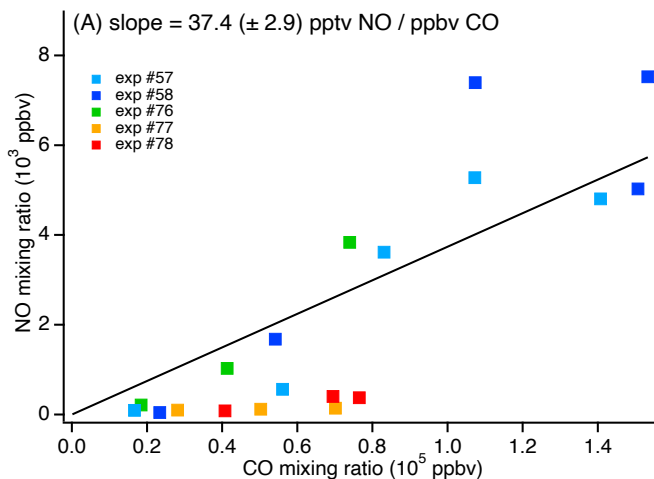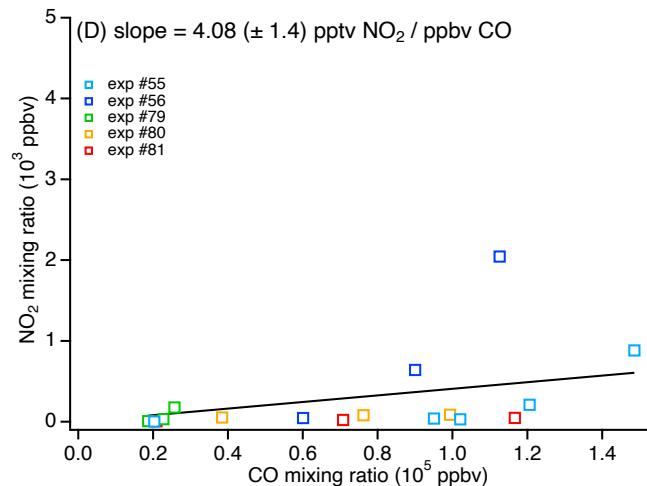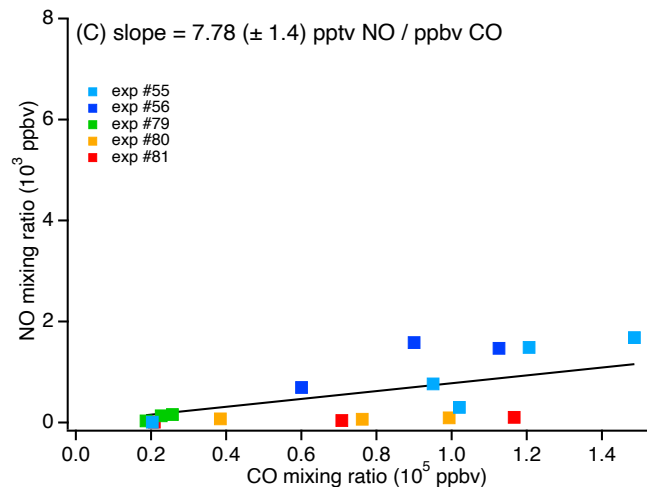
Figure S6. NO and NO₂ concentrations (ppbv) as a function of CO (ppbv). Graphs (A-B) correspond to the ceramic brakes while graphs (C-D) are for the semi-metallic brakes. Individual experiments per brake types are represented by a different color to highlight the variability across experiments. Data are missing for exp #8 and #9 because the NO/NO₂ analyzer was not available. The slope of these plots is defined as the emission ratio (ER).
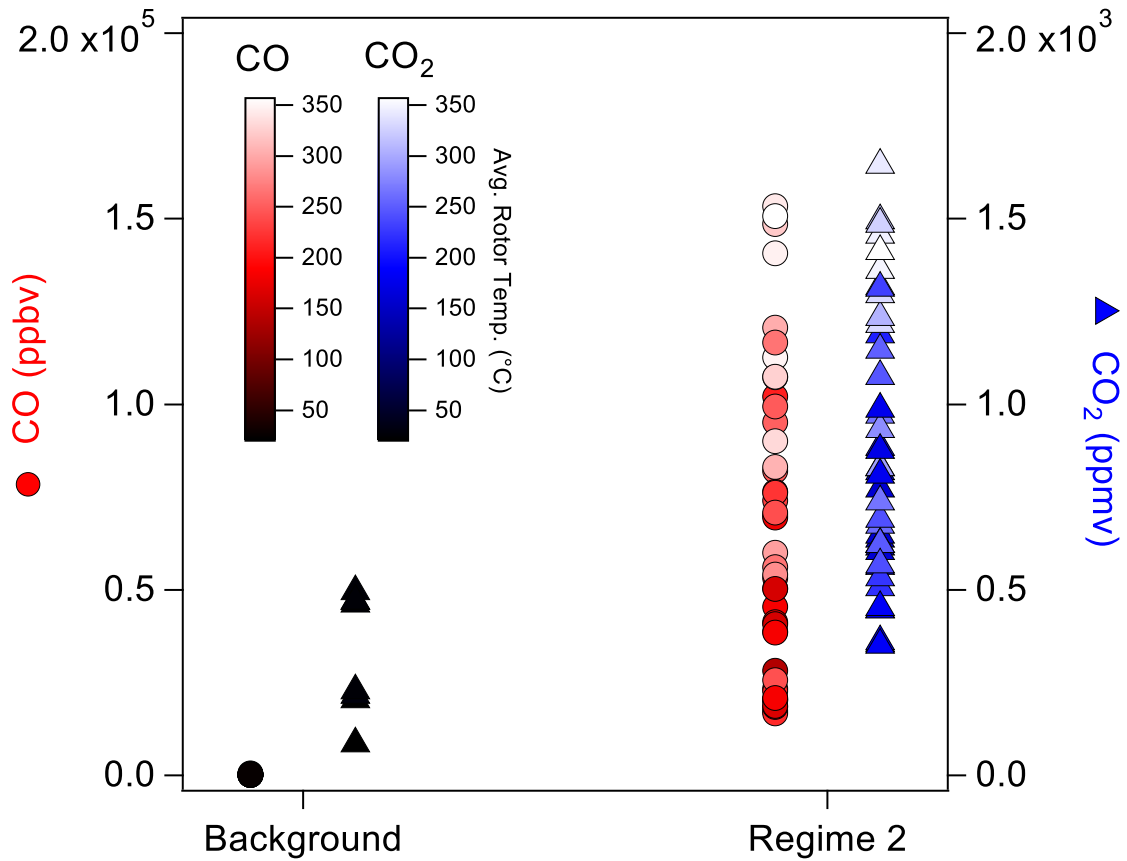
Figure S7. Mixing ratios of CO (red data points, ppbv) and CO_2 (blue data points, ppmv) measured during all ceramic and semi-metallic brake dynamometer experiments in regime 2. Background CO (black circles) and CO_2 (black triangles) mixing ratios measured when the lathe was off at the beginning of each experiment are also plotted for reference.
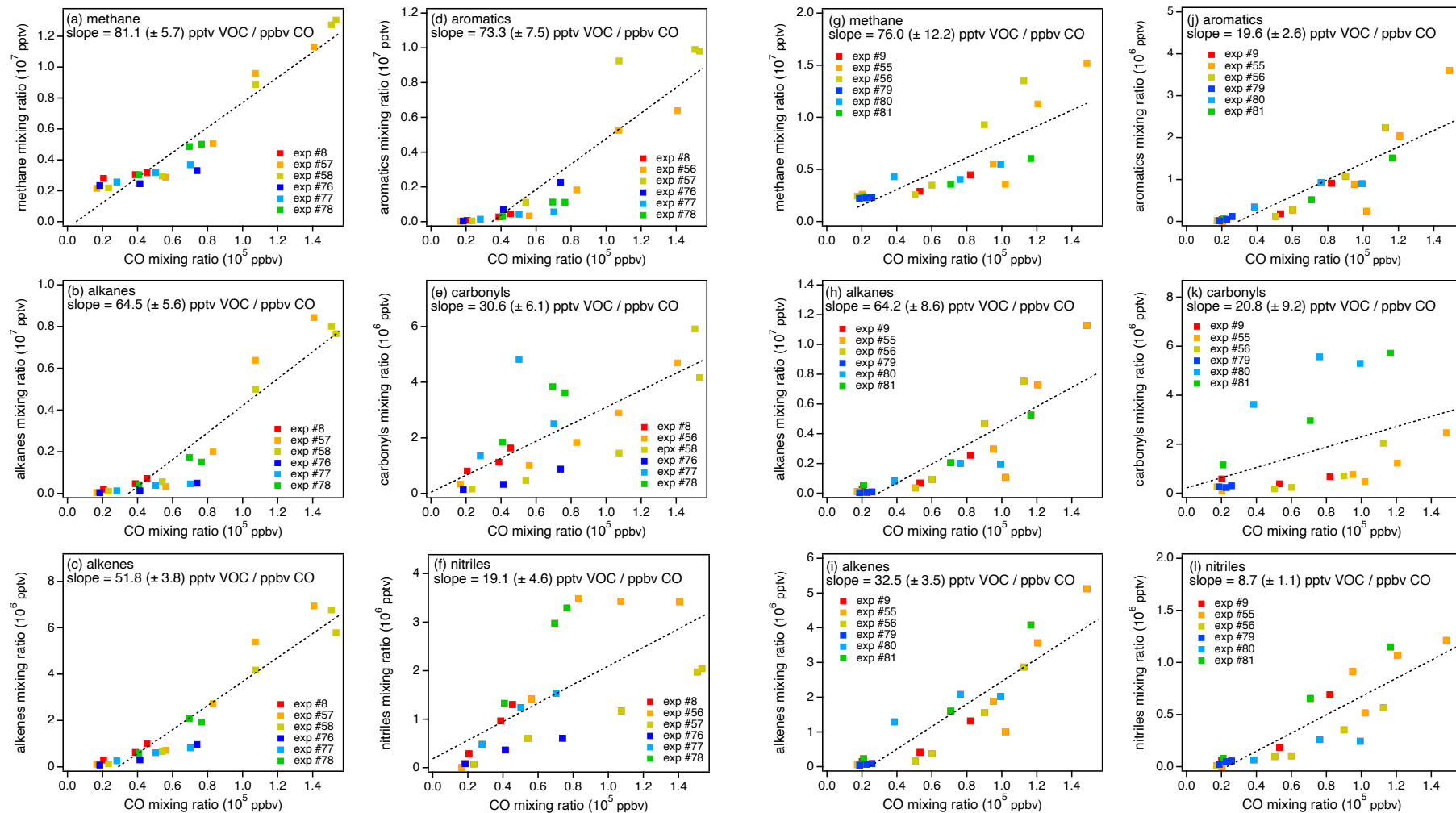
Figure S8. Typical plots of VOC concentration (pptv) versus CO concentration (ppbv). The VOC were classified in 13 chemical categories. Note that the alkane category does not include CH_4 but methane is plotted separately (graph (a) and (g)). Graphs (a-f) correspond to ceramic brakes while graphs (g-l) are for semi-metallic brakes. All six experiments per brake type are represented by a

different color to highlight the variability across experiments. The slope of these plots is defined as the emission ratio (ER) of the chemical family and the distribution of the experimentally determined emissions ratios are presented in Fig. 2.
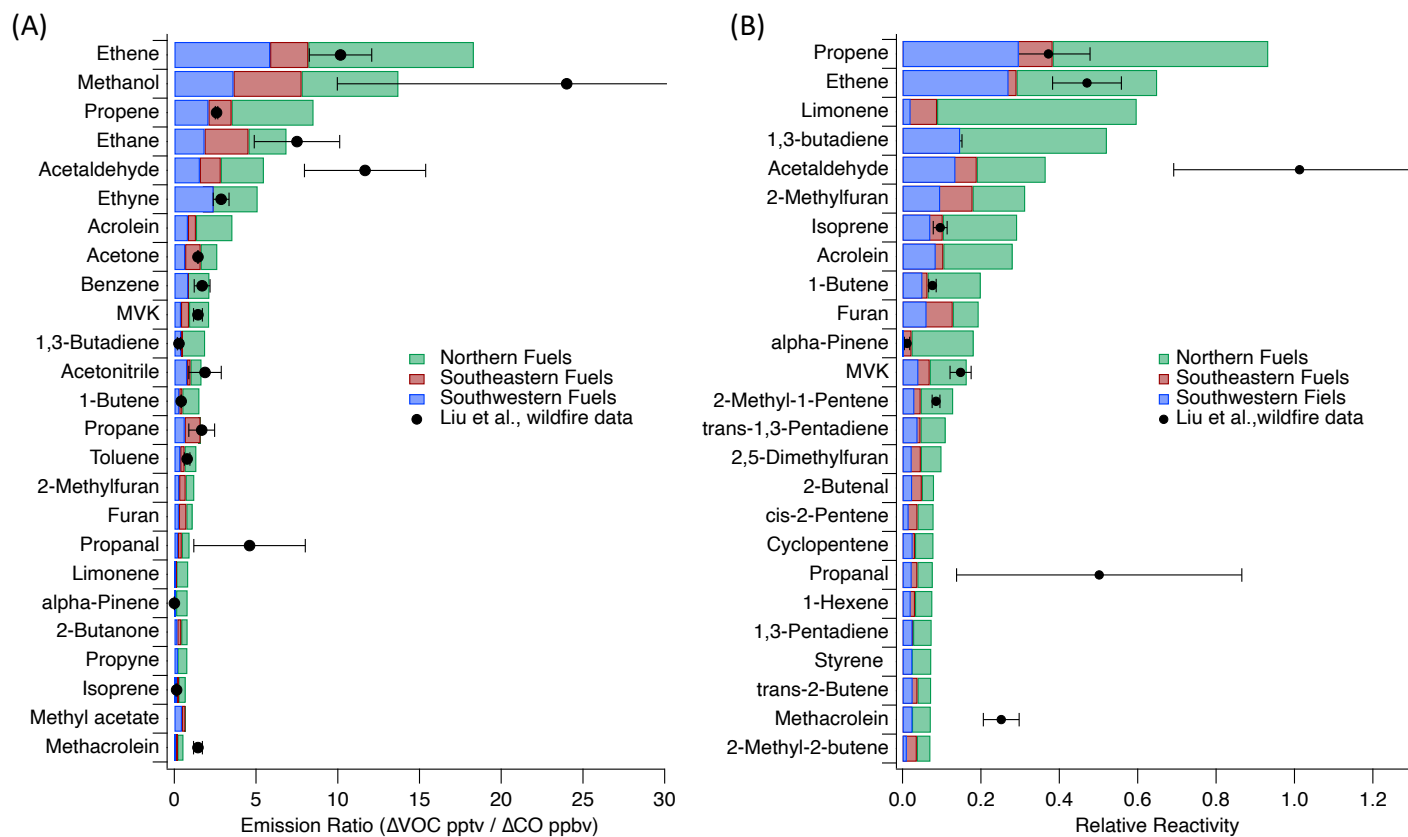
Figure S9. **Average emission ratios and relative reactivity of individual VOC (top 25) relative to CO from biomass burning emissions.** (**A**) Average emission ratios from laboratory biomass burning studies for combustion of some fuels characteristic of the north (N), southeast (SE) and southwest (SW) regions of the United States[20] and (**B**) relative reactivity of individual VOC from the same studies as (A). Note that in (A), the colored bars are overlays of the total emission ratios for each region. For example, for ethene the ERs are 18, 8 and 6 for N, SE and SW fuels, respectively. The filled circles represent wildfire data and reactivity estimated based on Liu et al.[21] Error bars for emission ratios represent one standard deviation and are used to determine the corresponding error in relative reactivity. ER values for methane (not displayed) are significantly higher than ethene and are off scale (ER = 40.9, 62.3 and 96.7 pptv/ppbv CO for the southwestern, southeastern and northern fuels respectively, and 96.0 pptv/ppbv CO for the wildfire study).
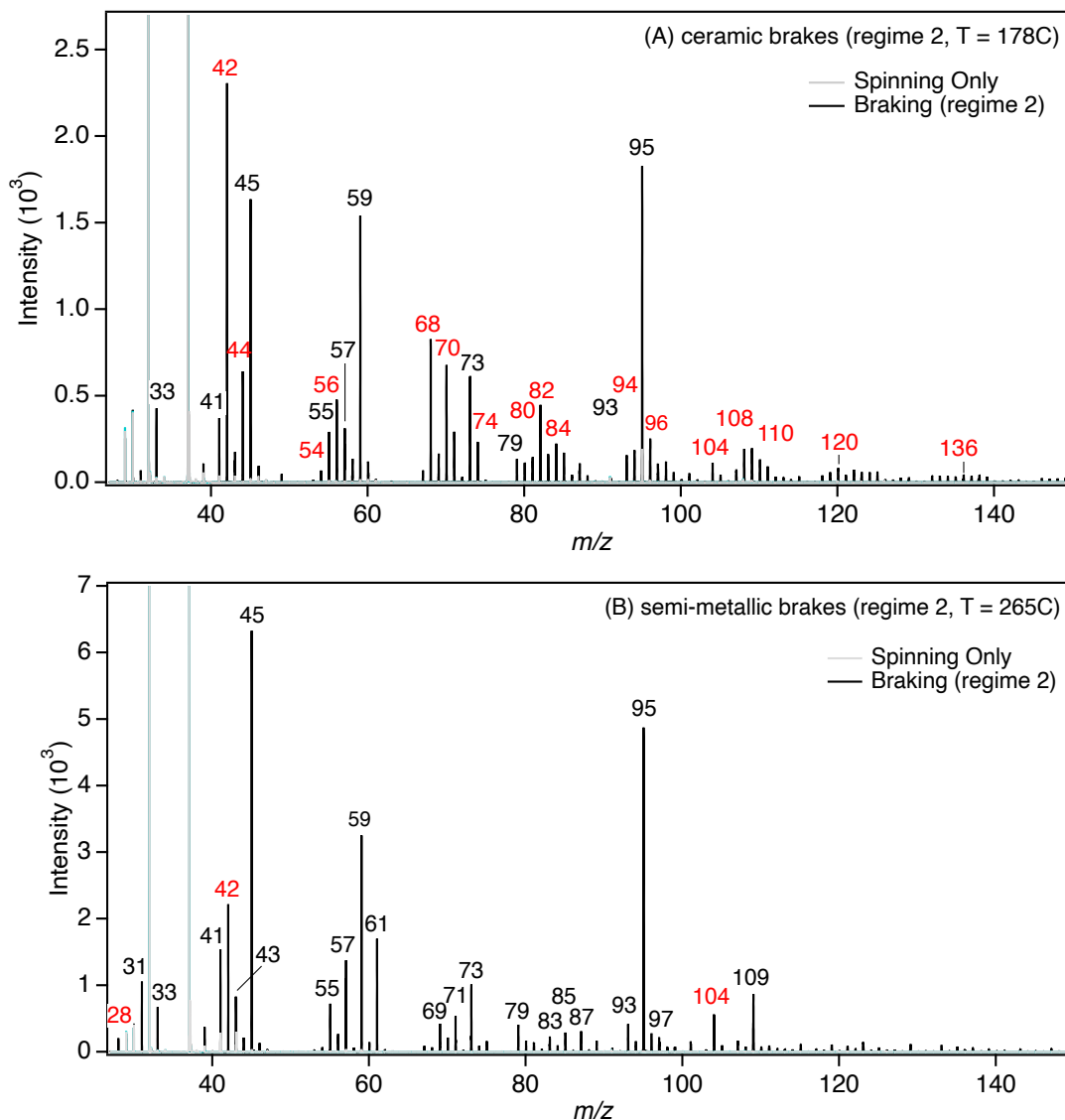
Figure S10. Typical PTR-MS spectra for gases emitted by brakes in regime 2. (**A**) MS spectra from a typical ceramic brake dynamometer experiment; (**B**) MS Spectra from a typical semi-metallic brake dynamometer experiment; The peaks marked in red are nitrogen-containing compounds. Peaks in light grey at *m/z* 32 and 37 are from O_2^+ and $(H_2O)H_3O^+$ ions, respectively, which are common to all spectra.
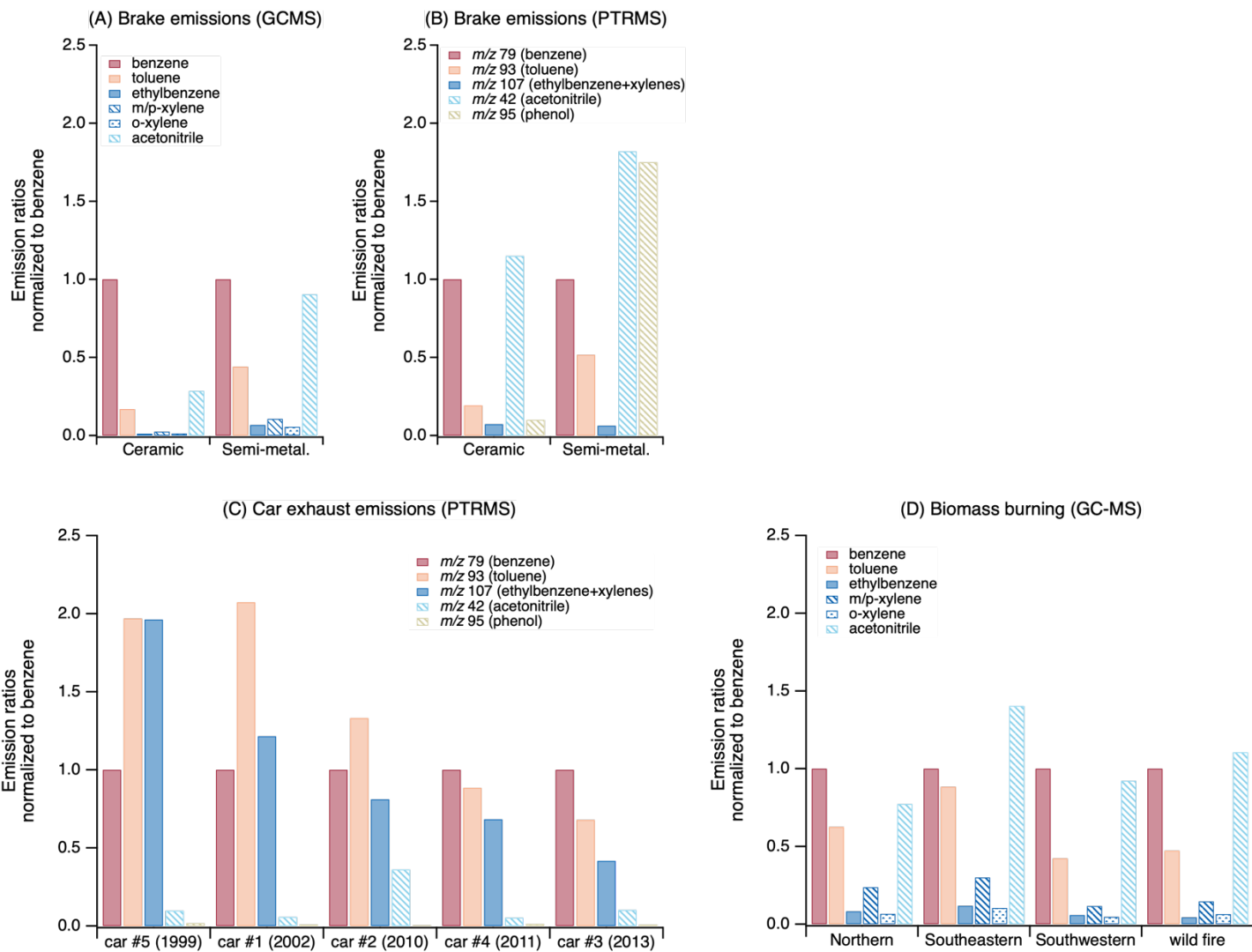
Figure S11. BTEX series measured in brake dynamometer experiments (regime 2) using either (A,B) the ceramic or semi-metallic brake pads compared with (C) tailpipe and (D) biomass burning measurements. Panels (A) and (D) show WAS

measurements while panels (B) and (C) shows PTR-MS measurements. The biomass burning measurements are from laboratory biomass burning studies for combustion of some fuels characteristic of the north (N), southeast (SE) and southwest (SW) regions of the United States[20] and from wildfire data from Liu et al.[21] The vehicles used in the tailpipe measurements include a 2002 Subaru WRX (car #1), a 2010 Honda Accord (car #2), a 2013 Hyundai Elantra (car #3), a 2011 Hyundai Santa Fe (car #4) and a 1999 Toyota Tacoma (car #5). Tailpipe measurements were performed at the exit of each tailpipe during a cold start while the cars were idling. In panels A and B, all VOC signals correspond to averaged emission ratios measured across six experiments normalized to that of benzene. Note that phenol could not be measured in the WAS canisters, however, its concentrations in exhaust are very small based on PTR-MS measurements at m/z 95. It was also not possible to differentiate ethylbenzene from the xylene isomers in the PTRMS, all producing a parent ion at m/z 107. As a consequence, although ethylbenzene is known to contribute some to the signal at m/z 79, all the signal measured at m/z 79 was attributed to benzene. The results from our small sample size of car exhaust emission were similar to those obtained from other tailpipe studies.[12-14]
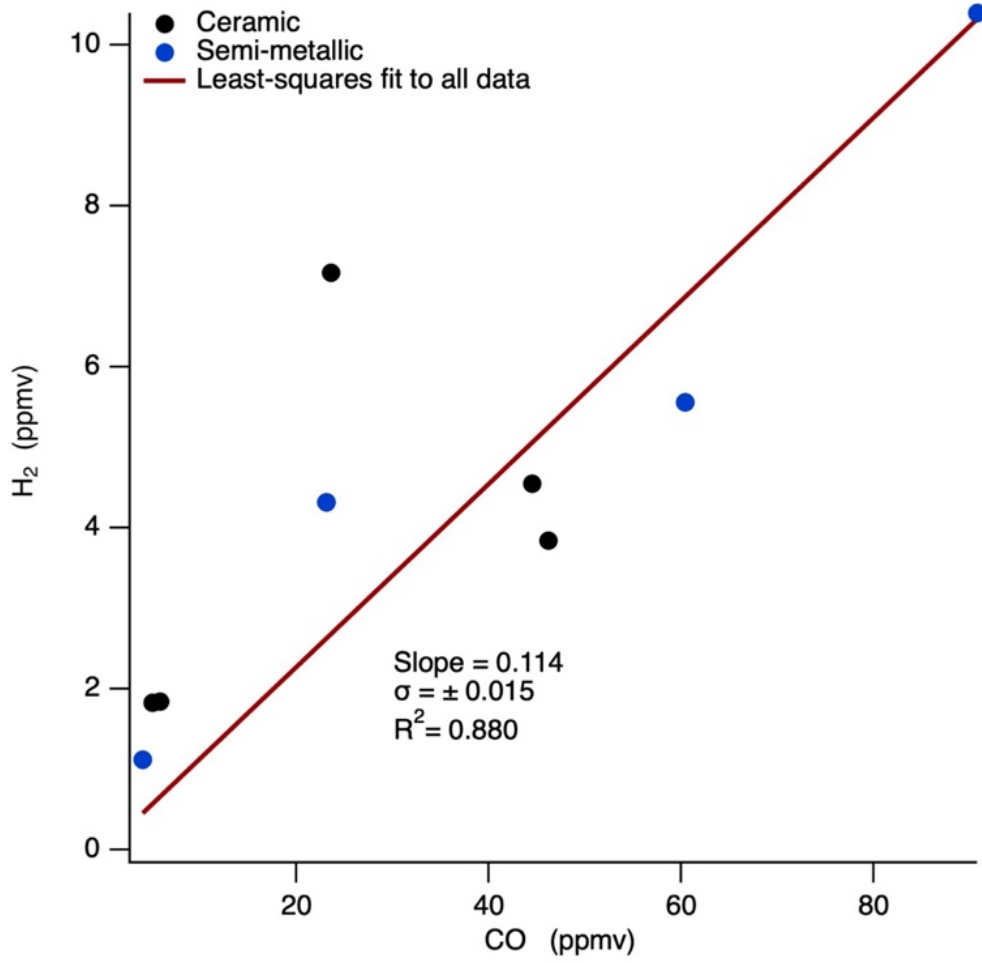
Figure S12. **H₂ mixing ratio versus CO mixing ratio measured from ceramic and semi-metallic brakes using the brake dynamometer (regime 2).**
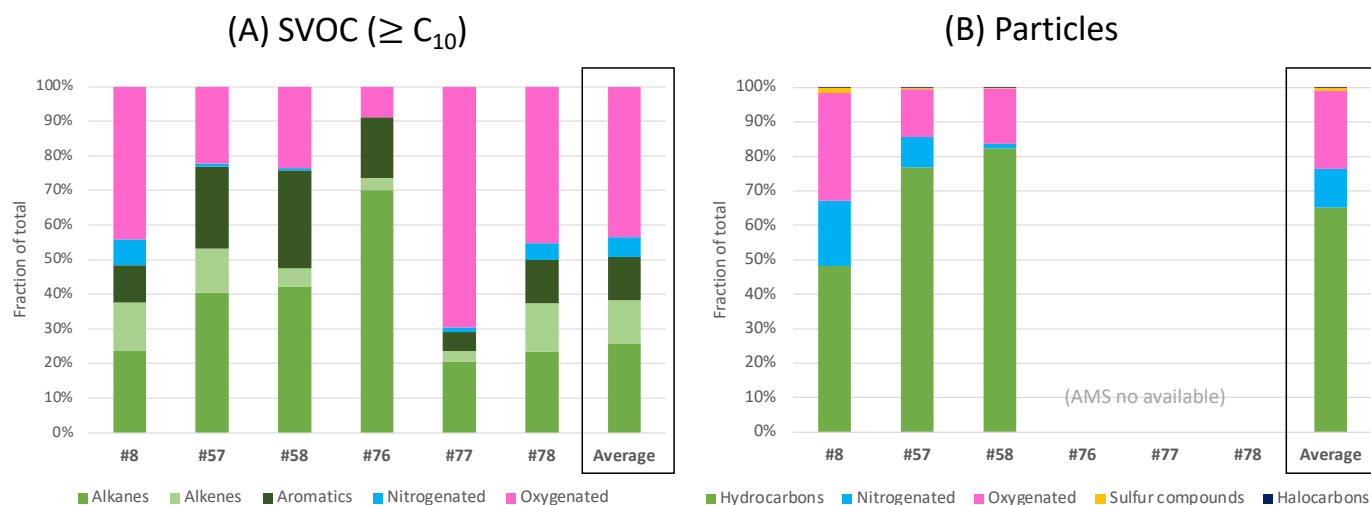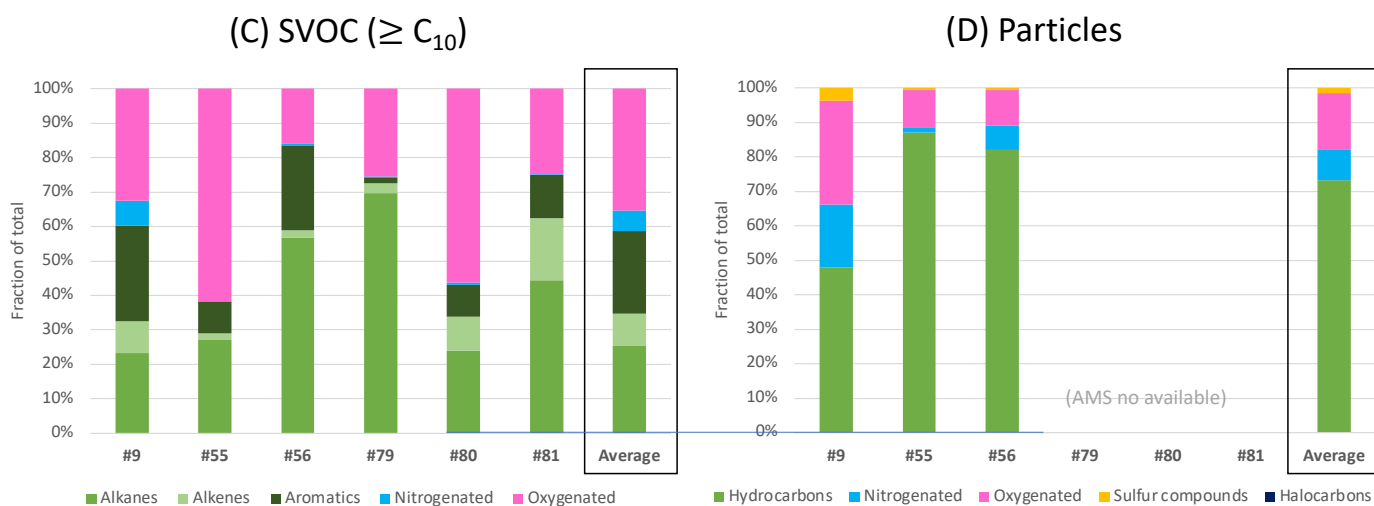
Figure S13. Semi-volatile organic compound distribution and particle chemical composition measured simultaneously for individual experiments with ceramic or semi-metallic brake pads under heavy braking conditions (regime 2). Mass distributions of (A) SVOC with 10 carbons or more and (B) particle components for ceramic brakes. Mass distributions of (C) SVOC with 10 carbons or more and (D) particle components for semi-metallic brakes. The trend in SVOC composition with each experiment is somewhat consistent with the particle composition, e.g. the trend in hydrocarbons in SVOC and particles for the first 3 experiments are similar. No sulfur-containing compounds were observed in the SVOC category, while in panels (B) and (D), sulfur compounds include $C_xH_yS_z^+$ as well as $HS_xO_y^+$ fragments. The charts in Figure 6 in the main text correspond to the averages shown here. Note that for exp #55 the largest difference observed between the SVOC ($\geq$ C10) and the AMS is the presence of glycol ethers possibly originating from brake fluid contributed to the oxygenated fraction of the

SVOCs measured. These glycols were not observed in significant amount in the PTR-MS measurements for this experiment. Additionally, for exp #77 and #80 (both experiments performed on a new brake), the large oxygenated fraction originates from C10 to C12 aldehydes and ketones rather than glycols.

Table S1. Emission ratios estimated for the ceramic and semi-metallic brake pads classified by family. The ER values correspond to the slope determined in the VOC vs CO plot (Fig. S8). Note that methane is excluded from the total VOC and percentage determination.

	Ceramic		Semi-metallic	
	ER	% of total VOC	ER	% of total VOC
	($\pm$1 std. dev.)		($\pm$1 std. dev.)	
Methane	81.1 ($\pm$5.7)	-	76.0 ($\pm$12.2)	-
Alkanes	64.5 ($\pm$5.6)	25	64.2 ($\pm$8.6)	40
Alkenes	51.8 ($\pm$3.8)	20	32.5 ($\pm$3.5)	20
Alkynes	2.3 ($\pm$0.2)	0.9	0.86 ($\pm$0.14)	0.5
Monoterpenes	6.4 ($\pm$2.2)	3	0.09 ($\pm$0.07)	0.05
Dienes	3.3 ($\pm$0.3)	1.3	0.84 ($\pm$0.14)	0.5
Aromatics	73.3 ($\pm$7.5)	29	19.6 ($\pm$2.6)	12
Carbonyls	30.6 ($\pm$6.1)	12	20.8 ($\pm$9.2)	13
Alcohols	0.50 ($\pm$2.5)	0.3	11.2 ($\pm$12.1)	7.0
Furans	1.8 ($\pm$0.3)	0.7	0.85 ($\pm$0.13)	0.5
Esters	0.03 ($\pm$0.07)	0.001	0.03 ($\pm$0.01)	0.02
Nitriles	19.1 ($\pm$4.6)	7	8.7 ($\pm$1.1)	5
S-compounds	0.96 ($\pm$0.11)	0.4	0.89 ($\pm$0.20)	0.6
Halogens	0.25 ($\pm$0.05)	0.10	0.31 ($\pm$0.06)	0.2

Table S2. Maximum rotor temperatures recorded for each brake type. Chamber temperatures are given in parentheses.

Ceramic Experiment No.	Rotor (chamber) temperature (°C)		Semi-metallic Experiment No.	Rotor (chamber) temperature (°C)	
	Regime 1	**Regime 2**		**Regime 1**	**Regime 2**
08	106 (48)	203 (64)	**09**	113 (48)	260 (60)
57 *	172 (54)	350 (83)	**55 ***	86 (44)	318 (69)
58 *	177 (58)	358 (89)	**56 ***	115 (47)	353 (77)
76 (old)	97 (49)	246 (66)	**79 (old)**	111 (44)	251 (61)
77 (new)	104 (44)	164 (54)	**80 (new)**	125 (44)	247 (56)
78 (new, day 2)	115 (49)	177 (58)	**81 (new, day 2)**	125 (44)	271 (59)

* These experiments were run for a longer time than the others, with regime 1 conditions maintained for ~63-65 min. (compared to 28-53 min.) and regime 2 maintained for 45-54 min. (compared to 27-43 min.)

Table S3. Weight percent of elements in brake particles from EDS analysis.

	Weight %	
Element	**Ceramic**	**Semi-metallic**
Fe	50.7	78.1
Ca	14.3	-
Mg	12.3	1.7
Si	8.7	12.4
Ba	4.2	5.4
K	4.0	-
Al	2.2	-
S	1.0	1.7
Other	2.7	0.8

Table S4. Emission ratios (expressed as pptv/ppbv), standard deviations and R^2 values for plots of each VOC (excluding methane) vs CO. All values are for ceramic brakes from WAS measurements in regime 2.

Ceramic VOC	ER	σ ER	σ ER/ ER	R^2	Ceramic VOC	ER	σ ER	σ ER/ ER	R^2
Ethene	13.625	0.862	6%	0.926	Benzene	55.195	7.411	13%	0.735
MAC	5.175	0.339	7%	0.921	n-Nonane	0.418	0.056	13%	0.733
Propene	11.370	0.761	7%	0.918	n-Decane	0.158	0.022	14%	0.728
2,2-Dimethylbutane	0.009	0.001	8%	0.892	Furan	0.452	0.064	14%	0.712
1-Pentene	1.486	0.116	8%	0.892	m/p-Xylene	1.336	0.204	15%	0.682
1-Butene	3.318	0.278	8%	0.877	Propanal	2.959	0.459	16%	0.675
Ethane	30.568	2.611	9%	0.873	1,2,3-Trimethylbenzene	0.811	0.128	16%	0.667
i-Butane	1.126	0.097	9%	0.872	3-Methylfuran	0.297	0.051	17%	0.665
Propane	14.585	1.276	9%	0.867	Benzofuran	0.921	0.148	16%	0.658
Ethyne	2.238	0.196	9%	0.867	beta-Pinene	0.075	0.013	17%	0.640
1-Hexene	1.029	0.091	9%	0.866	Cyclohexane	0.094	0.016	17%	0.632
n-Octane	0.879	0.077	9%	0.866	2,3-Dimethylpentane	0.034	0.006	17%	0.631
o-Xylene	0.694	0.062	9%	0.863	1,2-Propadiene	0.050	0.009	18%	0.609
3-Methyl-1-butene	0.171	0.016	9%	0.857	MVK	1.153	0.208	18%	0.605
Toluene	9.317	0.857	9%	0.855	Benzonitrile	2.736	0.537	20%	0.605
1-Heptene	0.449	0.041	9%	0.855	Ethylbenzene	0.648	0.132	20%	0.546
1,3,5-Trimethylbenzene	0.317	0.029	9%	0.855	Acetone	10.863	2.318	21%	0.523
Cyclopentane	0.246	0.023	9%	0.852	trans-1,3-Pentadiene	0.184	0.042	23%	0.492
cis-2-Pentene	0.333	0.031	9%	0.852	alpha-Pinene	0.300	0.070	24%	0.475
i-Pentane	0.476	0.044	9%	0.851	Acetone + Propanal	23.961	9.696	40%	0.466
i-Butene	13.986	1.311	9%	0.851	Acetonitrile	15.736	3.869	25%	0.453
cis-2-Butene	0.988	0.094	10%	0.847	1-Butyne	0.017	0.005	27%	0.410
2-Methylpentane	0.228	0.022	10%	0.846	Acrylonitrile	0.119	0.037	31%	0.372
2-Methyl-1-Butene	0.673	0.064	10%	0.845	Propyne	0.068	0.021	31%	0.343
n-Butane	6.431	0.617	10%	0.844	Limonene	5.994	2.102	35%	0.289
Isoprene	2.681	0.259	10%	0.843	Cyclopentene	0.202	0.073	36%	0.274
trans-2-Pentene	0.652	0.064	10%	0.840	Acetaldehyde	5.696	2.482	44%	0.208
n-Heptane	1.658	0.165	10%	0.835	Isopropanol	0.269	0.221	82%	0.175
trans-2-Butene	1.416	0.141	10%	0.835	i-Propylbenzene	0.045	0.022	49%	0.175
n-Pentane	3.956	0.397	10%	0.832	Styrene	0.224	0.111	50%	0.169
Methylcyclopentane	0.486	0.049	10%	0.832	1,3-Butadiene	0.389	0.211	54%	0.145
3-Methylpentane	0.077	0.008	10%	0.827	4-Methyl-1-pentene	0.056	0.038	68%	0.101
2,2,4-Trimethylpentane	0.164	0.017	10%	0.822	2-Methylpropanal	0.371	0.322	87%	0.062
Methylcyclohexane	0.169	0.018	10%	0.820	n-Propylbenzene	0.074	0.067	91%	0.057
4-Ethyltoluene	1.352	0.144	11%	0.815	Methyl acetate	0.001	0.002	137%	0.026
3-Methylhexane	0.188	0.020	11%	0.809	Butanal	0.218	0.317	145%	0.023
n-Hexane	2.484	0.274	11%	0.804	2-Methylfuran	0.109	0.172	158%	0.020
2-Methyl-2-butene	1.054	0.117	11%	0.804	Propanenitrile	0.477	0.801	168%	0.017
1-Octene	0.995	0.110	11%	0.802	2,5-Dimethylfuran	0.020	0.037	186%	0.017
Acrolein	3.822	0.431	11%	0.797	cis-1,3-Pentadiene	0.017	0.037	215%	0.011
3-Ethyltoluene	0.616	0.073	12%	0.782	Butanone	0.301	0.849	282%	0.006
2-Methylhexane	0.084	0.010	12%	0.777	2,3-Dimethylbutane	0.00003	0.00038	1500%	0.00030
1,2,4-Trimethylbenzene	1.850	0.226	12%	0.770	Methanol	0.584	2.268	388%	0.003
Chlorobenzene	0.126	0.016	12%	0.766	Ethanol	-0.058	0.249	-432%	0.003
2-Ethyltoluene	0.715	0.095	13%	0.741	Anisole	-0.003	0.087	-2636%	0.000
Continued…									

Table S5. Emission ratios (expressed as pptv/ppbv), standard deviations and R^2 values for plots of each VOC (excluding methane) vs CO. All values are for semi-metallic brakes from WAS measurements in regime 2.

Semi-metallic VOC	ER	σ ER	σ ER/ ER	R^2	Semi-metallic VOC	ER	σ ER	σ ER/ ER	R^2
1,3-Butadiene	0.382	0.037	10%	0.843	3-Methylpentane	0.090	0.019	21%	0.534
Propene	7.414	0.748	10%	0.831	m/p-Xylene	0.909	0.192	21%	0.528
Ethene	10.693	1.182	11%	0.804	2-Ethyltoluene	0.407	0.095	23%	0.479
Acrylonitrile	0.049	0.006	13%	0.790	1,3,5-Trimethylbenzene	0.122	0.030	24%	0.458
n-Butane	7.103	0.823	12%	0.788	Acrolein	1.616	0.408	25%	0.440
2,2,4-Trimethylpentane	0.118	0.014	12%	0.782	3-Ethyltoluene	0.388	0.100	26%	0.431
n-Pentane	3.967	0.485	12%	0.769	1,2,3-Trimethylbenzene	0.740	0.191	26%	0.429
Toluene	3.772	0.469	12%	0.764	Ethylbenzene	0.574	0.149	26%	0.425
1-Butene	2.847	0.358	13%	0.760	1-Pentene	1.424	0.374	26%	0.420
Cyclohexane	0.086	0.015	17%	0.754	1,2,4-Trimethylbenzene	1.257	0.331	26%	0.418
Cyclopentane	0.157	0.020	13%	0.750	4-Ethyltoluene	1.138	0.301	26%	0.416
i-Butene	4.485	0.589	13%	0.744	n-Nonane	0.384	0.105	27%	0.399
Propane	15.254	2.020	13%	0.740	Isoprene	0.232	0.064	28%	0.397
Acetonitrile	7.733	1.043	13%	0.733	trans-1,3-Pentadiene	0.176	0.053	30%	0.391
trans-2-Butene	1.154	0.158	14%	0.728	n-Decane	0.155	0.046	30%	0.361
cis-2-Butene	0.779	0.107	14%	0.727	Cyclopentene	0.193	0.059	30%	0.353
Propanenitrile	0.595	0.082	14%	0.723	Anisole	0.027	0.010	35%	0.332
3-Methylfuran	0.046	0.007	15%	0.722	3-Methyl-1-butene	0.127	0.040	32%	0.331
cis-2-Pentene	0.241	0.035	14%	0.707	1-Hexene	0.941	0.300	32%	0.329
2,2-Dimethylbutane	0.008	0.001	14%	0.705	Chlorobenzene	0.114	0.036	32%	0.328
2-Methyl-1-Butene	0.234	0.036	15%	0.677	1-Heptene	0.452	0.158	35%	0.325
trans-2-Pentene	0.495	0.076	15%	0.677	carbon disulfide	0.095	0.032	34%	0.307
o-Xylene	0.473	0.074	16%	0.671	Isopropanol	0.139	0.082	59%	0.293
i-Butane	1.012	0.159	16%	0.670	2-Methylfuran	0.116	0.041	36%	0.282
Methylcyclohexane	0.137	0.022	16%	0.667	Acetone	3.983	1.470	37%	0.269
i-Pentane	0.377	0.060	16%	0.666	Acetaldehyde	9.315	3.441	37%	0.268
Benzonitrile	0.390	0.070	18%	0.662	MAC	0.698	0.302	43%	0.211
2-Methylhexane	0.058	0.009	16%	0.657	2,5-Dimethylfuran	0.039	0.019	50%	0.201
Benzene	8.553	1.415	17%	0.646	alpha-Pinene	0.028	0.012	45%	0.200
Methylcyclopentane	0.376	0.062	17%	0.646	Methyl acetate	0.008	0.004	47%	0.187
2-Methyl-2-butene	0.441	0.076	17%	0.626	Propyne	0.014	0.006	47%	0.186
1-Octene	0.529	0.106	20%	0.624	beta-Pinene	-0.005	0.002	-48%	0.181
2-Methylpentane	0.190	0.034	18%	0.617	1-Butyne	0.045	0.022	49%	0.173
Ethane	28.583	5.041	18%	0.616	Propanal	1.684	0.846	50%	0.166
2,3-Dimethylpentane	0.027	0.005	18%	0.608	n-Propylbenzene	0.224	0.118	53%	0.152
Ethyne	0.801	0.145	18%	0.603	Styrene	0.870	0.544	63%	0.113
i-Propylbenzene	0.042	0.008	18%	0.599	2-Methylpropanal	0.557	0.381	68%	0.097
n-Heptane	2.651	0.486	18%	0.598	2,3-Dimethylbutane	0.005	0.003	72%	0.088
3-Methylhexane	0.129	0.024	19%	0.590	Butanone	0.228	0.198	87%	0.062
MVK	0.272	0.052	19%	0.579	cis-1,3-Pentadiene	0.034	0.034	102%	0.060
n-Hexane	2.791	0.539	19%	0.573	Methanol	7.144	7.304	102%	0.046
Furan	0.328	0.064	19%	0.571	4-Methyl-1-pentene	0.052	0.060	115%	0.041
Benzofuran	0.336	0.069	20%	0.569	Ethanol	4.046	4.713	116%	0.036
n-Octane	0.606	0.118	20%	0.567	Limonene	0.058	0.068	117%	0.035
Methyl Chloride	0.273	0.055	20%	0.549	1,2-Propadiene	0.003	0.008	262%	0.007
Dimethyl sulfide	0.016	0.003	19%	0.544	Butanal	0.264	0.955	361%	0.004
Continued…									

Table S6. Gas phase rate constants (cm^3 molecule^{-1} s^{-1}) for the reactions of OH with the VOC identified from brake emissions.[22-27] All rate constants are given at room temperature to evaluate the reactivity of each VOC once it is emitted in ambient air.

VOC	$10^{12}k_{OH}$	VOC	$10^{12}k_{OH}$	VOC	$10^{12}k_{OH}$
Limonene	171	1-Pentene	31.4		
2,5-Dimethylfuran	130	Methacrolein	31.4	Toluene	6.00
2-Ethylfuran	110	4-Methyl-1-pentene	38.0	n-Hexane	5.45
trans-1,3-Pentadiene	105	3-Methyl-1-butene	31.8	Methylcyclopentane	5.66
cis-1,3-Pentadiene	101	Propene	26.3	2,3-Dimethylpentane	5.10
Isoprene	101	Butanal	25.5	Cyclopentane	4.84
3-Methylfuran	93.0	Vinyl acetate	24.9	Carbon disulfide	4.70
2-Methyl-2-butene	87.0	2-Methylpropanal	23.0	2-Pentanone	4.05
Cyclopentene	67.0	Propanal	20.0	Acrylonitrile	4.04
trans-2-pentene	66.8	3-Ethyltoluene	19.2	n-Pentane	4.00
1,3-Butadiene	66.6	Acrolein	19.0	Ethanol	3.20
cis-2-Pentene	65.1	m/p-Xylene	19.0	3-Pentanone	2.90
trans-2-Butene	63.7	MVK	18.5	n-Butane	2.33
2-Methylfuran	62.0	Acetaldehyde	16.0	iso-Butane	2.19
2-Methyl-1-Pentene	62.0	p-Cymene	15.7	2-Butanone	1.20
2-Methyl-1-butene	61.0	o-Xylene	13.7	Benzene	1.20
1,1-Dimethylhydrazine	60.3	n-Undecane	12.9	Propane	1.12
1,3,5-Trimethylbenzene	57.5	2-Ethyltoluene	12.3	Methanol	0.930
cis-2-Butene	56.4	4-Ethyltoluene	12.1	Ethyl Formate	0.850
alpha-Pinene	53.7	n-Decane	11.2	Methyl Propanoate	0.830
Styrene	52.0	n-Nonane	10.3	Ethyne	0.770
iso-Butene	51.4	n-Octane	8.70	Benzonitrile	0.330
Furan	42.0	Ethene	8.52	Methyl acetate	0.320
1-Heptene	40.0	n-Heptane	7.18	Propanenitrile	0.256
Benzofuran	37.2	Ethylbenzene	7.10	Ethane	0.254
1-Hexene	37.0	2-Methylhexane	6.86	Acetone	0.220
1,2,4-Trimethylbenzene	36.7	3-Methylhexane	6.72	Methyl Formate	0.170
2-Butenal	36.4	Cyclohexane	7.21	Methyl Chloride	0.034
1-Octene	33.0	Dimethyl sulfide	6.50	Acetonitrile	0.022
1,2,3-Trimethylbenzene	32.7	3-Methylpentane	5.20	Methane	0.0062
1-Butene	31.4	Propyne	6.06	Carbonyl sulfide	0.0020
Continued …		Continued …			

Table S7. PTR-MS high resolution peak identification: major ions identified in both brake types[a]

m/z	Formulae	Potential ID
18.034	NH_4^+	ammonia
28.021	$HCNH^+$	hydrogen cyanide
31.021	CH_3O^+	formaldehyde
33.036	CH_5O^+	methanol (WAS ID)[a]
39.026	$C_3H_3^+$	frag.[b] alkanes & alkenes
41.041	$C_3H_5^+$	frag. alkanes & alkenes
42.046	$C_2H_4N^+$	acetonitrile (WAS ID)
43.020	$C_2H_3O^+$	acetic acid frag.
43.057	$C_3H_7^+$	frag. alkanes & alkenes
44.016	$HNCOH^+$	isocyanic acid
44.052	$C_2H_6N^+$	ethenamine
45.034	$C_2H_5O^+$	acetaldehyde (WAS ID)
46.029	CH_4NO^+	formamide
46.068	$C_2H_8N^+$	ethylamine
47.016	$CH_3O_2^+$	formic acid
47.049	$C_2H_7O^+$	ethanol (WAS ID)[c]
49.013	CH_5S^+	methanethiol
54.038	$C_3H_4N^+$	acrylonitrile (WAS ID)
55.057	$C_4H_7^+$	1,3-butadiene/butyne (WAS ID); frag. alkanes & alkenes
56.053	$C_3H_6N^+$	propanenitrile (WAS ID)
57.037	$C_3H_5O^+$	acrolein (WAS ID)
57.072	$C_4H_9^+$	butene (WAS ID); frag. alkenes & alkanes
58.068	$C_3H_8N^+$	propenamine
59.052	$C_3H_7O^+$	acetone/propanal (WAS ID)
60.044	$C_2H_6NO^+$	acetamide
60.082	$C_3H_{10}N^+$	trimethylamine
61.031	$C_2H_5O_2^+$	acetic acid
63.028	$C_2H_7S^+$	dimethylsulfide (WAS ID)
63.044	$C_2H_7O_2^+$	ethanediol
67.054	$C_5H_7^+$	cyclopentadiene
68.050	$C_4H_6N^+$	pyrrole
69.037	$C_4H_5O^+$	furan (WAS ID)
69.071	$C_5H_9^+$	isoprene
70.067	$C_4H_8N^+$	butanenitrile
71.054	$C_4H_7O^+$	methacrolein/MVK (WAS ID)
71.085	$C_5H_{11}^+$	frag. alkene & alkanes
73.031	$C_3H_5O_2^+$	methyl glyoxal
73.069	$C_4H_9O^+$	butanal/butanone/methylpropanal (WAS ID)
74.060	$C_3H_8NO^+$	dimethylformamide
75.046	$C_3H_7O_2^+$	methyl acetate (WAS ID);
79.056	$C_6H_7^+$	benzene (WAS ID)
80.051	$C_5H_6N^+$	pyridine
81.045	$C_4H_5N_2^+$	pyrazine
81.071	$C_6H_9^+$	frag. terpenes
82.068	$C_5H_8N^+$	methylpyrrole + isomers
83.053	$C_5H_7O^+$	methylfuran (WAS ID)
83.085	$C_6H_{11}^+$	hexadiene/cyclohexene

84.084	$C_5H_{10}N^+$	pentanenitrile (=valeronitrile)
85.069	$C_5H_9O^+$	methylbutenal/methylbutenone/pentenal
85.101	$C_6H_{13}^+$	frag. alkanes & alkenes
87.047	$C_4H_7O_2^+$	butanedione/butyrolactone
87.083	$C_5H_{11}O^+$	pentanal(-one)/methylbutanal(-one)
93.072	$C_7H_9^+$	toluene (WAS ID)
94.066	$C_6H_8N^+$	aniline/methylpyridine
95.053	$C_6H_7O^+$	phenol
96.081	$C_6H_{10}N^+$	ethylpyrrole
97.030	$C_5H_5O_2^+$	furfural
97.067	$C_6H_9O^+$	C2 substituted furans (WAS ID)
97.101	$C_7H_{13}^+$	frag. alkene & alkanes (heptanal)
98.100	$C_6H_{12}N^+$	methylpentanenitrile/hexanenitrile
99.084	$C_6H_{11}O^+$	hexenal/cyclohexanone/methylcyclopentanone
101.060	$C_5H_9O_2^+$	methylmethacrylate
101.097	$C_6H_{13}O^+$	hexanal/hexanone
104.054	$C_7H_6N^+$	benzonitrile (WAS ID)
105.071	$C_8H_9^+$	styrene (WAS ID)
107.053	$C_7H_7O^+$	benzaldehyde
107.086	$C_8H_{11}^+$	xylenes/ethylbenzene (WAS ID)
108.082	$C_7H_{10}N^+$	C2 substituted pyridine
109.030	$C_6H_5O_2^+$	p-benzoquinone
109.065	$C_7H_9O^+$	anisole (WAS ID)
109.099	$C_8H_{13}^+$	cyclooctadiene
110.098	$C_7H_{12}N^+$	C3 substituted pyrroles
111.083	$C_7H_{11}O^+$	C3 substituted furans
115.113	$C_7H_{15}O^+$	heptanal/heptanone
118.067	$C_8H_8N^+$	indole
119.054	$C_8H_7O^+$	benzofuran (WAS ID)
119.085	$C_9H_{11}^+$	indane/methylstyrene
120.083	$C_8H_{10}N^+$	dihydropyridine
121.068	$C_8H_9O^+$	tolualdehyde/acetophenone
121.102	$C_9H_{13}^+$	C3 substituted benzene (WAS ID)
122.098	$C_8H_{12}N^+$	C3 substituted pyridine + isomers
123.047	$C_7H_7O_2^+$	hydroxybenzaldehyde
123.086	$C_8H_{11}O^+$	C2 substituted phenols
124.113	$C_8H_{14}N^+$	C4 substituted pyrroles + isomers
125.097	$C_8H_{13}O^+$	butylfuran + isomers
129.079	$C_{10}H_9^+$	naphthalene
129.127	$C_8H_{17}O^+$	octanal/octanone
133.070	$C_9H_9O^+$	methylbenzofuran
135.114	$C_{10}H_{15}^+$	C4 substituted benzene
136.023	$C_7H_6NS^+$	benzothiazole
136.114	$C_9H_{14}N^+$	C4 substituted pyridine + isomers
137.131	$C_{10}H_{17}^+$	monoterpenes

Brake fluid ions[d]

89.0568	$C_4H_9O_2^+$	diethylene glycol fragment
107.070	$C_4H_{11}O_3^+$	diethylene glycol
149.115	$C_7H_{17}O_3^+$	ethanol, 2-(2-propoxyethoxy)-
163.126	$C_8H_{19}O_3^+$	diethylene glycol monobutyl ether

| 179.122 | $C_8H_{19}O_4^+$ | triethylene glycol monoethyl ether |
| 207.156 | $C_{10}H_{23}O_4^+$ | triethylene glycol monobutyl ether |

[a]Compounds also identified by WAS indicated with blue notation.

[b]frag = fragment of parent compound

[c]Inomata et al. (2009) reported that ethanol fragments into H_3O^+ at higher E/N conditions, such as the ones used in this study (~135 Td). Consequently, the sensitivity at *m/z* 47 is reduced. This was confirmed with an authentic standard. It is impossible to quantify the fragment ion, as a result, ethanol concentration using exclusively *m/z* 47 is underestimated (Fig. 5).

[d]Ions associated with the brake fluid were observed in the PTRMS mass spectra as the temperature increased during regime 2 but were relatively small in most experiments. Note that some contribution of brake fluid to *m/z* 45 cannot be excluded. Glycol ether identification was based on a MSDS report of DOT 3 brake fluid.[28]

References

1. J. J. Colman, A. L. Swanson, S. Meinardi, B. C. Sive, D. R. Blake, F. S. Rowland, Description of the analysis of a wide range of volatile organic compounds in whole air samples collected during PEM-Tropics A and B, *Anal. Chem.,* 2001, **73**, 3723-3731.
2. C. L. Faiola, M. H. Erickson, V. L. Fricaud, B. T. Jobson, T. M. VanReken, Quantification of biogenic volatile organic compounds with a flame ionization detector using the effective carbon number concept, *Atmos. Meas. Tech.,* 2012, **5**, 1911-1923.
3. A. Jordan, S. Haidacher, G. Hanel, E. Hartungen, L. Märk, H. Seehauser, R. Schottkowsky, P. Sulzer, T. D. Märk, A high resolution and high sensitivity proton-transfer-reaction time-of-flight mass spectrometer (PTR-TOF-MS), *Int. J. Mass Spectrom.,* 2009, **286**, 122-128.
4. M. Graus, M. Müller, A. Hansel, High Resolution PTR-TOF: Quantification and Formula Confirmation of VOC in Real Time, *J. Am. Soc. Mass. Spectrom.,* 2010, **21**, 1037-1044.
5. C. E. Stockwell, P. R. Veres, J. Williams, R. J. Yokelson, Characterization of biomass burning emissions from cooking fires, peat, crop residue, and other fuels with high-resolution proton-transfer-reaction time-of-flight mass spectrometry, *Atmos. Chem. Phys.,* 2015, **15**, 845-865.
6. A. Hansel, A. Jordan, R. Holzinger, P. Prazeller, W. Vogel, W. Lindinger, Proton-transfer reaction mass-spectrometry - Online trace gas-analysis at the ppb level, *Int. J. Mass Spectrom.,* 1995, **149**, 609-619.
7. R. Holzinger, J. Williams, F. Herrmann, J. Lelieveld, N. M. Donahue, T. Röckmann, Aerosol analysis using a Thermal-Desorption Proton-Transfer-Reaction Mass Spectrometer (TD-PTR-MS): a new approach to study processing of organic aerosols, *Atmos. Chem. Phys.,* 2010, **10**, 2257-2267.
8. W. Lindinger, A. Hansel, A. Jordan, On-line monitoring of volatile organic compounds at pptv levels by means of proton-transfer-reaction mass spectrometry (PTR-MS) - Medical applications, food control and environmental research, *Int. J. Mass Spectrom.,* 1998, **173**, 191-241.
9. R. Holzinger, W. J. F. Acton, W. J. Bloss, M. Breitenlechner, L. R. Crilley, S. Dusanter, M. Gonin, V. Gros, F. N. Keutsch, A. Kiendler-Scharr, L. J. Kramer, J. E. Krechmer, B. Languille, N. Locoge, F. Lopez-Hilfiker, D. Materic, S. Moreno, E. Nemitz, L. L. J.

Quéléver, R. S. Esteve, S. Sauvage, S. Schallhart, R. Sommariva, R. Tillmann, S. Wedel, D. R. Worton, K. M. Xu, A. Zaytsev, Validity and limitations of simple reaction kinetics to calculate concentrations of organic compounds from ion counts in PTR-MS, *Atmos. Meas. Tech.,* 2019, **12**, 6193-6208.

10. D. Pagonis, K. Sekimoto, J. de Gouw, A library of proton-transfer reactions of H_3O^+ Ions used for trace gas detection, *J. Am. Soc. Mass. Spectrom.,* 2019, **30**, 1330-1335.

11. J. Zhao, R. Y. Zhang, Proton transfer reaction rate constants between hydronium ion (H_3O^+) and volatile organic compounds, *Atmos. Environ.,* 2004, **38**, 2177-2185.

12. G. T. Drozd, Y. L. Zhao, G. Saliba, B. Frodin, C. Maddox, R. J. Weber, M. C. O. Chang, H. Maldonado, S. Sardar, A. L. Robinson, A. H. Goldstein, Time resolved measurements of speciated tailpipe emissions from motor vehicles: trends with emission control technology, cold start effects, and speciation, *Environ. Sci. Technol.,* 2016, **50**, 13592-13599.

13. A. H. Goldstein, A. Robinson, J. Kroll, G. T. Drozd, Y. H. Zhao, G. Saliba, R. Saleh, A. Presto (2017) Investigating semi-volatile organic compound emissions from light-duty vehicles. (California Air Resources Board Report,), pp 1-225.

14. B. Marques, E. Kostenidou, A. M. Valiente, B. Vansevenant, T. Sarica, L. Fine, B. Temime-Roussel, P. Tassel, P. Perret, Y. Liu, K. Sartelet, C. Ferronato, B. D'Anna, Detailed speciation of non-methane volatile organic compounds in exhaust emissions from diesel and gasoline Euro 5 vehicles using online and offline measurements, *Toxics,* 2022, **10**, Art No 184, doi: 110.3390/toxics10040184.

15. J. K. Jiang, C. M. Kim, X. L. Wang, M. R. Stolzenburg, S. L. Kaufman, C. L. Qi, G. J. Sem, H. Sakurai, N. Hama, P. H. McMurry, Aerosol charge fractions downstream of six bipolar chargers: effects of ion source, source activity, and flowrate, *Aerosol Sci. Technol.,* 2014, **48**, 1207-1216.

16. A. Miller, G. Frey, G. King, C. Sunderman, A Handheld electrostatic precipitator for sampling airborne particles and nanoparticles, *Aerosol Sci. Technol.,* 2010, **44**, 417-427.

17. P. F. DeCarlo, J. R. Kimmel, A. Trimborn, M. J. Northway, J. T. Jayne, A. C. Aiken, M. Gonin, K. Fuhrer, T. Horvath, K. S. Docherty, D. R. Worsnop, J. L. Jimenez, Field-deployable, high-resolution, time-of-flight aerosol mass spectrometer, *Anal. Chem.,* 2006, **78**, 8281-8289.

18. Y. L. Chen, L. Xu, T. Humphry, A. P. S. Hettiyadura, J. Ovadnevaite, S. Huang, L. Poulain, J. C. Schroder, P. Campuzano-Jost, J. L. Jimenez, H. Herrmann, C. O'Dowd, E. A. Stone, N. L. Ng, Response of the aerodyne aerosol mass spectrometer to inorganic sulfates and organosulfur compounds: applications in field and laboratory measurements, *Environ. Sci. Technol.,* 2019, **53**, 5176-5186.

19. D. K. Farmer, A. Matsunaga, K. S. Docherty, J. D. Surratt, J. H. Seinfeld, P. J. Ziemann, J. L. Jimenez, Response of an aerosol mass spectrometer to organonitrates and organosulfates and implications for atmospheric chemistry, *P Natl Acad Sci USA,* 2010, **107**, 6670-6675.

20. J. B. Gilman, B. M. Lerner, W. C. Kuster, P. D. Goldan, C. Warneke, P. R. Veres, J. M. Roberts, J. A. de Gouw, I. R. Burling, R. J. Yokelson, Biomass burning emissions and potential air quality impacts of volatile organic compounds and other trace gases from fuels common in the US, *Atmos. Chem. Phys.,* 2015, **15**, 13915-13938.

21. X. X. Liu, L. G. Huey, R. J. Yokelson, V. Selimovic, I. J. Simpson, M. Muller, J. L. Jimenez, P. Campuzano-Jost, A. J. Beyersdorf, D. R. Blake, Z. Butterfield, Y. Choi, J. D.

Crounse, D. A. Day, G. S. Diskin, M. K. Dubey, E. Fortner, T. F. Hanisco, W. W. Hu, L. E. King, L. Kleinman, S. Meinardi, T. Mikoviny, T. B. Onasch, B. B. Palm, J. Peischl, I. B. Pollack, T. B. Ryerson, G. W. Sachse, A. J. Sedlacek, J. E. Shilling, S. Springston, J. M. St Clair, D. J. Tanner, A. P. Teng, P. O. Wennberg, A. Wisthaler, G. M. Wolfe, Airborne measurements of western US wildfire emissions: Comparison with prescribed burning and air quality implications, *J. Geophys. Res.,* 2017, **122**, 6108-6129.

22. R. Atkinson, Kinetics and mechanisms of the gas-phase reactions of the hydroxyl radical with organic compounds under atmospheric conditions, *Chem. Rev.,* 1986, **86**, 69-201.

23. R. Atkinson, A structure-activity relationship for the estimation of rate constants for the gas-phase reactions of OH radicals with organic-compounds, *Int. J. Chem. Kinet.,* 1987, **19**, 799-828.

24. B. J. Finlayson-Pitts, J. N. Pitts, Jr., *Chemistry of the Upper and Lower Atmosphere - Theory, Experiments, and Applications* (Academic Press, San Diego, 2000), pp. 969.

25. J. A. Manion, R. E. Huie, R. D. Levin, D. R. Burgess Jr., V. L. Orkin, W. Tsang, W. S. McGivern, J. W. Hudgens, V. D. Knyazev, D. B. Atkinson, E. Chai, A. M. Tereza, C.-Y. Lin, T. C. Allison, W. G. Mallard, F. Westley, J. T. Herron, R. F. Hampson, D. H. Frizzell (2015) NIST Chemical Kinetics Database, NIST Standard Reference Database 17, version 7.0 (web version), release 1.6.8, Data version 2015.09. (National Institute of Standards and Technology, Gaithersburg, Maryland, 20899-8320).

26. M. M. Sprengnether, K. L. Demerjian, T. J. Dransfield, J. S. Clarke, J. G. Anderson, N. M. Donahue, Rate constants of nine C6-C9 alkanes with OH from 230 to 379 K: chemical tracers for [OH], *Journal of Physical Chemistry A,* 2009, **113**, 5030-5038.

27. M. B. Blanco, I. Bejan, I. Barnes, P. Wiesen, M. A. Teruel, Atmospheric oxidation of vinyl and allyl acetate: product distribution and mechanisms of the OH-initiated degradation in the presence and absence of NO, *Environ. Sci. Technol.,* 2012, **46**, 8817-8825.

28. Complex Chemical Co (2015) MSDS for DOT 3 brake fluid. pp 1-6.